Discrete element simulation of powder layer spreading by blade sliding: packing factor, mechanism, and optimization

L. Dai[1,a], Y.R. Chan[2], G. Vastola[1], Y.W. Zhang[1,b]

[1] *Institute of High Performance Computing (IHPC), Agency for Science, Technology and Research (A*STAR), 1 Fusionopolis Way, #16-16 Connexis, 138632, Singapore*
[2]*Advanced Remanufacturing and Technology Centre (ARTC), Agency for Science, Technology and Research (A*STAR), 3 Cleantech Loop, #01/01 CleanTech Two, 637143, Singapore*

Abstract

We utilized the Discrete Element Method (DEM) to simulate the packing of a powder layer by blade spread. Our study revealed the following findings: (1) We uncovered a hereditary relationship that exists between the pouring heap and the packing layer, which plays a significant role in the non-uniform distribution of powder in the packing layer in terms of sizes and shapes. (2) We systematically analysed the influence of sliding speed on powder packing and recommended a threshold sliding rate of 0.15 m/s for achieving a high packing quality. (3) Contrary to the conventional belief that non-spherical powders tend to reduce packing density, our study discovered that the inclusion of a small portion of non-spherical powders can create pathways for efficient gap-filling, resulting in denser packings. (4) By adjusting inter-powder interactions, we observed a transition from discrete powder packing to cluster deposition. (5) We proposed and demonstrated the efficacy of a two-step spreading technique followed by multiple shaking cycles in achieving maximum random packing density. Overall, our work provides a comprehensive understanding of mechanisms involved in the powder spreading process through blade sliding, which may lead to enhanced powder packing density and uniformity and ultimately improved outcomes in additive manufacturing.

1. Introduction

Powder bed fusion additive manufacturing (AM), in which a part is built layer-by-layer by selectively melting and solidifying the powder layers, has attracted enormous attention in both academia and industry [1]. An important step in AM is the formation of a powder layer, in which powders are being spread by a sliding blade. The high packing quality of the powder layer, i.e., high packing density and uniformity, is crucial for the quality of final AM products [2-4]. Hence, significant efforts have been devoted to achieving high packing density and

[a] Email: dail@ihpc.a-star.edu.sg
[b] Email: zhangyw@ihpc.a-star.edu.sg

uniformity. Besides experimental characterizations, computer simulations have also been used in the development of powder spreading, especially the Discrete Element Method (DEM) [5, 6], which has been proven to be a powerful tool to reproduce the spreading process by means of modelling the physical properties of powders and dynamics [7, 8].

Mindt et al. [9] performed DEM simulations on multi-layer powder deposition and layer build-up. Their study showed that the powder packing layer needed sufficient height to avoid discrete packing, which was well correlated with the porosity measured after build-up, as reported by Li and Mizutani [10]. The experimental characterizations by Nan et al. [11, 12] indicated that without sufficient layer height, the individual powders could be dragged by the blade, which could, in turn, trigger large vacancies. Based on DEM simulations, Han et al. proposed an optimized powder layer height, which was slightly higher than the averaged diameter of powders, typically around 30-50μm [13]. On the other hand, experimental study by Wischeropp et al. [14] suggested that the optimized height of the powder packed layer should be around 4-5.5 times of the build-up layer, which was also validated by the work from Liu et al. [15] and Mahmoodkhani et al. [16]. Moreover, the uniformity of the spreading layer is also an important factor affecting the printing quality as it could cause rough surface after the build-up. It is known that the uniformity of powder packing is affected by the blade sliding speed and the imposed load from the blade as reported by Parteli et al. [17].

Besides packing height, the flowability of individual powders is a fundamentally important factor that affects packing density and uniformity [18, 19] because highly flowable powders are more likely to fill the vacancy sites to enhance the packing density [20-22]. However, flowability is a physical quantity that can be influenced by many factors, including powder size [23-26], shape [27, 28], interaction [29-33], blade sliding speed [34, 35] et al. For example, Haeri et al. [36, 37] reported that a larger aspect ratio of powders with low flowability, and a higher blade sliding speed decreased the packing density, while a geometry change to a roller blade could improve the packing density. In addition, Chen et al. reported that small powders can be generally beneficial to the powder flowability, but too fine powders (radius < 21.8μm in their settings) could cause a strong cohesion, and thus an unfavourable powder packing [38]. The negative effect from powder cohesion was also studied and presented [39]. Generally, a fast blade sliding speed was found to spread powders loosely onto the plate, resulting in a lower packing density [40]. He et al. [41] studied the combined effects of powder size and cohesion, and found that a better layer quality could be obtained either by small powders with a weak interface cohesion or large powders with a moderate interface cohesion, whilst a strong interface cohesion always led to a sparse and non-uniform powder layer due to reduced flowability. Similar findings for the effects from those factors, including powder size,

shape, friction, cohesion, layer height, and blade sliding speed, et al., were also reported in many other studies [21, 33, 42-45].

Studies from Fouda and Bayly [46] indicated that the packing density of a powder layer was generally lower than that of its initial powder heap counterpart, and three mechanisms were identified: (1) shear-induced dilation during the initiation of powder motion by sliding blade; (2) dilation and rearrangement due to powder motion through the gap; and (3) the inertia of the powders in the deposited powder layer. The packing density and uniformity were also reported to be correlated with non-mean distribution of powder size along the blade sliding process [47]. Much as reported, the mechanisms for the lower packing density in the powder layer, and the relationship between the powder pouring heap and the flat powder packing layer have not been well understood. Furthermore, it is well-known that packing fraction (PF), which is defined as the ratio of the volume occupied by powders to the volume of the enclosed geometry, is typically around 0.56-0.64 [48] for a natural and random powder packing. Clearly, there is a strong need to gain an in-depth understanding in the effects from different factors, that is, the powder properties and spreading process conditions, which can guide the rational manipulation of powders to achieve high packing density and uniformity, motivates the present work.

In this work, we perform DEM simulations to study the powder spreading process by considering different influencing factors, aiming to present an in-depth, comprehensive understanding in the powder spreading process, reveal their underlying mechanisms, and explore the guidelines for improving the powder packing quality.

2. Methodology

An in-house DEM simulation package in C++ language was developed to model, run and post-process the simulations. We chose the popular Inconel718 [49] as our powder material. As presented in our previous experimental work [50], Inconel718 powders were purchased from GE Additive [51], and the powder size and shape were characterized by Malvern Morphologi G3 machine with the AMI-SOP-017 procedure. Based on the measured high sensitivity (HS) circularity [27] and aspect ratio [52], around 90% powders were highly spherical particles with a diameter distribution of 13μm, 30μm and 52μm for D10, D50 and D90, respectively. The D10, D50 and D90 stand for the particle size such that 10% of the total particles have diameters no more than D10=13μm; 50% of particles have diameters no more than D50=30μm; and 90% particles have diameters no more than D90=52μm. The remaining powders included 5% satellite (STL) shape, which was composed of two sticked spherical particles, and 5% ellipsoid (EPD) shape. In this report, we use the word “particle” specially for the

simple spherical granules, while we use the word "powder" as a general term to include spherical particles as well as non-spherical granules.

Following the experimental characterizations in our previous literature [50], we set up the standard DEM powder model as 90-5-5, which was composed of 90% particles, 5% STL and 5% EPD non-spherical powders. Besides, we also designed two additional models, i.e., 40-30-30 (40% particles, 30% STL and 30% EPD non-spherical powders) and particle (100% particle) models for comparison. The quantities for each powder model were shown in Table-1. In each model, the diameter of spherical particles always followed a Gaussian distribution between 10μm to 55μm, and a mean-value of 30μm, to mimic the experimental measurements as D10, D50 and D90 [50]. As shown in Fig.1, different colours were assigned to indicate the size difference of the particles. The chart-(a) in Fig.1 showed some representative experimental snapshots of non-spherical powders, and the numerical approach by clump of particles. Based on experimental observations, the STL powders were modelled as two sticked particles, for which the diameters of the two constituent particles were randomly picked from the distribution of spherical particles. EPD powders were set up by clumping five partially overlapping constituent particles, and categorized into two sub-types with distinct particle diameters in this sequence: 30μm-34μm-38μm-34μm-30μm and 18μm-22μm-26μm-22μm-18μm for the from left to right. The intrinsic properties, such as the mass, moment of inertia, were calculated by integrating the constituent particles. For the non-spherical powders, the constituent particles were treated individually when computing their interactions but treated as a rigid block when performing the linear movement or rotation.

The simulation model was also presented in Fig.1. The whole model had a lateral span of 2mm along X-axis, which was divided into a trash zone, a working zone and a pouring zone separated by wall-1 and wall-2. Wall-1 and wall-2 were located at 0mm and 1.25mm, respectively, along the X-axis and had an identical height of 0.15mm along Y-axis, which was 5 times as the averaged diameter of spherical particles. This height was shown to be suitable for powder packing [15]. The periodical boundary condition was applied along Z-axis (perpendicular to the XY plane). The whole model had a period of 1.25mm along Z-axis, thus forming a 0.25mm x 1.25mm area (the XZ plane) for the trash zone, a 1.25mm x 1.25mm area for the working zone, and 0.5mm x 1.25mm for the pouring zone. The size of working zone was suitable to hold a packing layer containing a few tens of thousands of powders. The pouring zone was confined by the pouring plate, which was located at 0.15mm height (along Y-axis), the wall-3 and the blade (see Fig.1). Initially, wall-3 served as the left boundary and the blade served as the right boundary for the pouring zone. Both the blade and wall-3 had a Y-dimension starting from 0.15mm to

infinitely upward. The model size and the quantity of powders used here were on the same scale with previous literatures and were validated as effective for numerical study [7, 11, 17].

The algorithms by Renzo [53, 54] and Ai [55] were used to describe the interactions and dynamics between powders and walls, for which the detail equations can be found in our previous work [50, 56]. The parameters for the dynamic simulations are shown in Table-2. It should be noted that conventional damping energy dissipation is a dynamic process during the period of collision. In order to include energy dissipation in DEM simulations, Kruggel-Emden et al. [57] have reviewed the algorithm and proposed that the normal collision force consists of two parts: one modelling the elastic repulsion and the other modelling the viscous dissipation. The viscous dissipation has an analytic solution derived by Schäfer et al. [58], leading to a constant coefficient of restitution (COR). Such application of constant COR has been widely adopted and validated in DEM simulations [59, 60]. Here, we adopt the value of COR from the work of Combarros et al. [59], which has been validated with reliable results [50]. The cohesion between two contacting particles is determined by surface energy, which has been thoroughly characterized in the work of Meier et al.[61] The values for the cohesion and four coefficients of friction (COF), i.e. $\mu_{pp\text{-}s}$ and $\mu_{pp\text{-}r}$ for sliding and rolling between two particles, and $\mu_{pw\text{-}s}$ and $\mu_{pw\text{-}r}$ for sliding and rolling between particle and wall, were adopted from our previous calibration [50], and will be tuned for parametrical analysis here. The standard blade sliding speed was set as 0.15m/s, and the tuning range between 0.01-0.5m/s, which is on the same scale as previous literature [34, 35, 44, 62]. The standard input parameters were applied in all simulations unless stated otherwise.

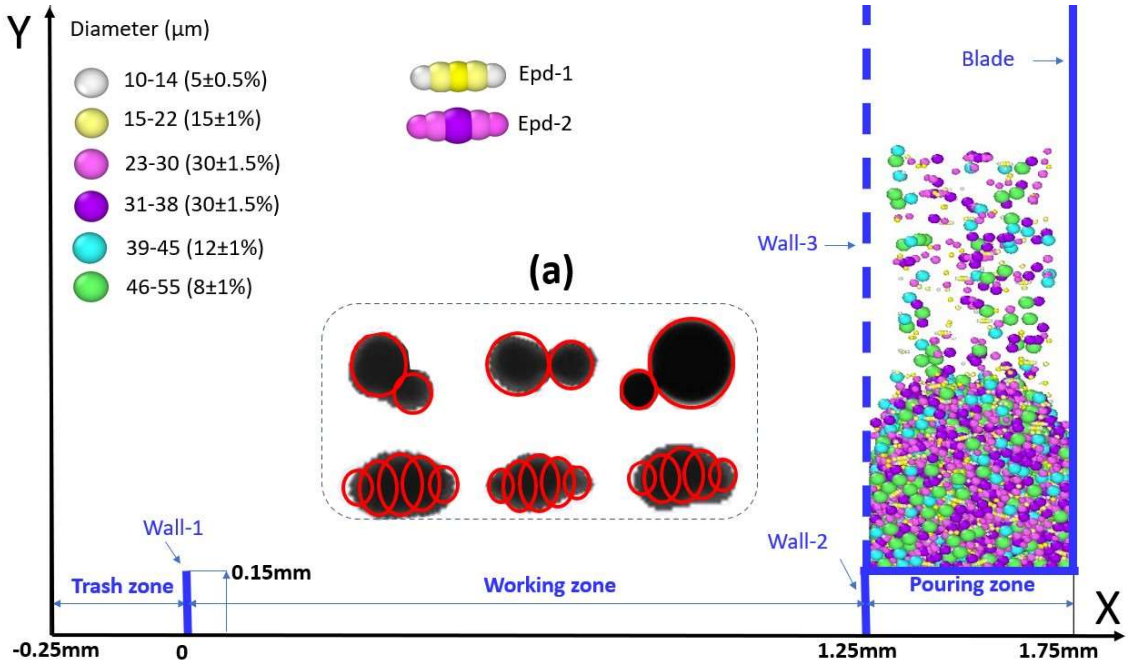

Fig.1. Front view of the simulation model and the individual powders. The diameters of particles were differentiated by color, together with mean and standard deviation of the size (Gaussian) distribution. The chart-(a) shows a few representative snapshots of individual non-spherical powders, i.e., STL and EPD, with clump-particle mimics.

Table-1. Quantities of powder for different models.

Model	Quantity
90-5-5 model	22,000
40-30-30 model	15,000
Particle model	25,000
small-particle in 90-5-5 model (particles with diameter 10-22μm)	20,000
non-small-powder in 90-5-5 model (particles with diameter >22μm)	12,000
small-particle in particle model (particles with diameter 10-22μm)	20,000
non-small-powder in particle model (particles with diameter >22μm)	14,000

Table-2. Parameters used in DEM simulations

Parameter	Standard Value
Young's modulus	205 GPa
Material density	8192 kg/m^3
Poisson ratio	0.22
Coefficient of restitution	0.75
Time step	1 ns
$\mu_{pp\text{-}s}$	0.39 (tuning 0.1-0.6)
$\mu_{pp\text{-}r}$	0.37 (tuning 0.1-0.6)
$\mu_{pw\text{-}s}$	0.05

$\mu_{pw\text{-}r}$	0.05
Cohesion (γ)	0.905 (tuning 0.1-3) mJ/m^2
Blade sliding speed	0.15 (tuning 0.05-0.5) m/s

Table-3. Definition of different powder groups.

Powder Group	Definition
small-particle	spherical particles with diameter 10-22μm
medium-particle	spherical particles with diameter 23-38μm
big-particle	spherical particles with diameter 39-55μm
non-sphere-powder	STL powders + EPD powders
heavy-powder	big-particle + non-sphere-powder
non-small-powder	medium-particle + big-particle + non-sphere-powder

The simulation started with a pouring stage, in which powders were created at a height of 0.7-0.9mm within the pouring zone. Under gravity, those created powders fell and formed a pouring heap on the pouring plate. Afterwards, wall-3 was removed, and the blade started to slide leftward at a pre-set constant speed to spread the powders onto the working plate until reaching the position right above wall-1. The remaining powders that were not deposited onto the working platform were discarded into the trash zone.

3. Results and discussion

3.1 Pouring heap

Firstly, the falling powders piled up to form a pouring heap on the pouring plate. Since the locations of individual powders within the pouring heap could determine the sequence of their spreading onto the working plate during the subsequent blade spread, the morphology of the pouring heap and the powder packing density and uniformity were worth analysing.

Fig.2 presented the views and measured powder quantities for the pouring heap of the 90-5-5 model. The pouring heap was vertically (along Y-axis) divided into six layers. Except the partially filled top (6th) layer, the other five individual layers were analysed, including the PF, average diameter (for spherical particles only), number of particles, STL and EPD powders, and plotted accordingly. Though the size and shape of powders were arbitrarily assigned upon initial powder creation, the distribution in the pouring heap showed an obvious segregation during their vertical stacking. Here, we defined different powder groups as shown in Table-3. In observation, the small-particles had the ability to re-locate and fill the gaps among other powders without changing the ambient morphology. The heavy-powders were observed to be able to squeeze neighbour powders aside during falling due to their heavy gravity, leading to re-construction of ambient morphology. Through by-layer counting,

there are more small-particles and heavy-powders in the lower layers of the pouring heap, while upper layers had more medium-particles. As shown in Fig.2, the numbers of non-sphere-powders, i.e., STL and EPD powders, were highest at layer-1 and decreased along stacking up. Due to the large quantity of small-particles passing downward through the gaps, the average diameter was smallest in layer-1. The gap-filling effect has been found to significantly enhance the PF [63] and the PF is the highest in the lowest layer, that is, layer-1, and gradually decreases with levelling up, as shown in Fig.2.

Fig.3 presented the views and measured powder quantities for the 40-30-30 pouring heap. The trend of the plots for PF, average diameter, numbers of spherical, STL and EPD powders, all were similar to those for the 90-5-5 model. The differences lie in the fact that 40-30-30 model had less particles, i.e., less small particles for gap-filling effect. Thus, in Fig.3, the average diameter of particles in layer-1 was larger for 40-30-30 model, due to less small-particles. Quantitatively, the values of PF were lower than those of the 90-5-5 model.

The analysis of the pouring heap for the particle model was presented in Fig.4. With solely particles, the trends of the plots for PF, average diameter, number of particle were still similar to the 90-5-5 and 40-30-30 models. Quantitatively, we noticed that among the three models, in layer-5, the PF for particle model was the highest while that for the 40-30-30 model was the lowest; but layer-1, the PF for the 90-5-5 model was the highest while that for the 40-30-30 model was still the lowest. Through additional simulations by tuning the powder size distribution, we found that if the gap-filling effect was excluded, the solely particle model would have the highest PF. In layer-5, the average diameter plot indicated that the small-particles were almost exhausted in the 90-5-5 and 40-30-30 models, so that the gap-filling effect was negligible. Therefore, the particle model recorded highest PF in layer-5. However, in layer-1, the involvement of non-sphere-powders brought more misfit among powders, which opened more paths for small particles to pass through. Therefore, in 90-5-5 model, the involvement of STL and EPD powders enhanced the PF by the gap-filling effect. Meanwhile, the insufficient quantity of small particles limited the gap-filling for 40-30-30 model.

As aforementioned, the segregation of different powder types were inevitable as far as there were size or shape distributions. Such segregation in the pouring stage was based on two mechanisms: 1) pass-filling vacancies by fine particles, and 2) gravity dragging on heavy powders. Similar segregation results of the pouring heap have also been reported in previous literatures (Combarros Garcia, Feise et al. 2016) and reviewed (Fan, Jacob et al. 2017). Such size and shape segregation in the pouring heap would strongly affect the density and uniformity of the packing layer in the subsequent blade spread process.

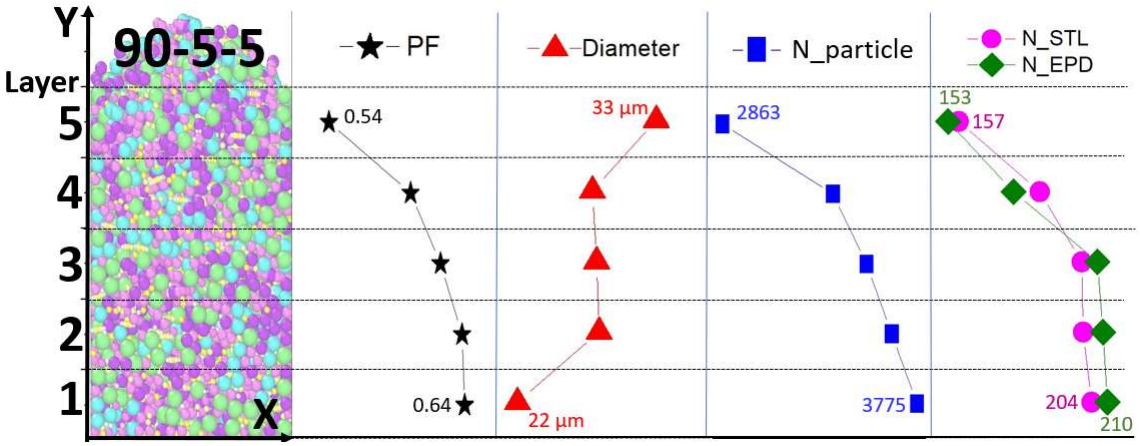

Fig.2. View of 90-5-5 pouring heap and layer-wise distribution of PF, average diameter, number of particles, STLs and EPDs, respectively.

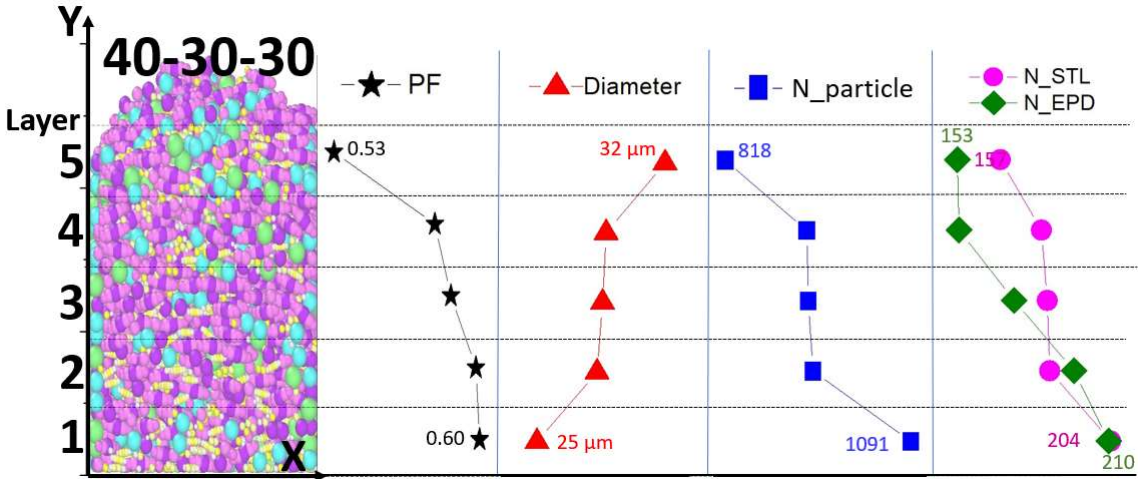

Fig.3. View of 40-30-30 pouring heap and layer-wise distribution of PF, average diameter, number of particles, STLs and EPDs, respectively.

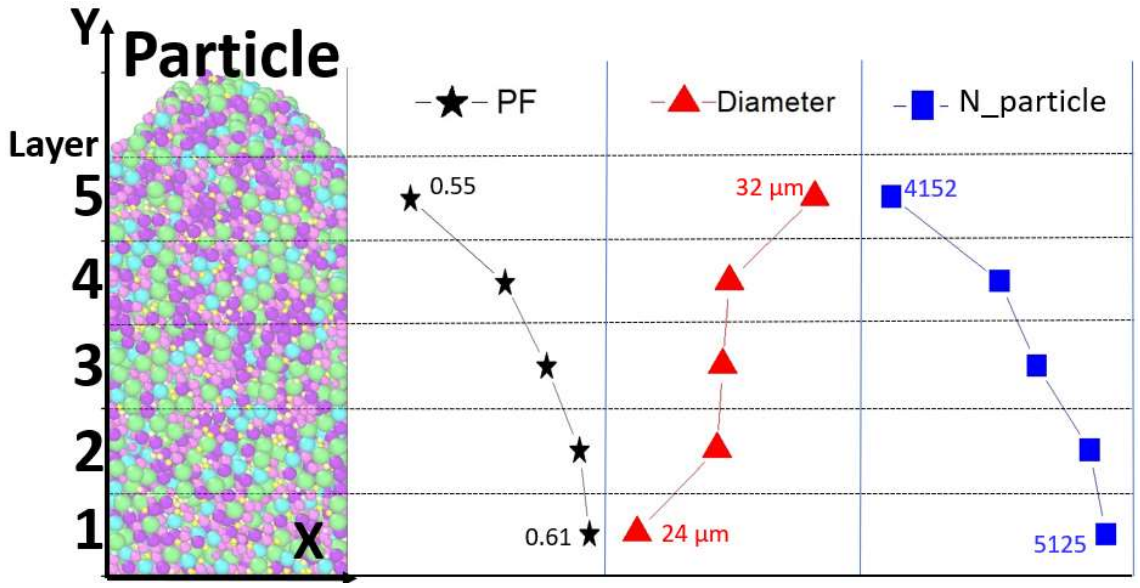

Fig.4. View of particle pouring heap and layer-wise distribution of PF, average diameter, number of particles, respectively.

3.2 Blade spread

After the stable pouring heap was formed, wall-3 was removed and at the same time, a constant velocity was assigned to the blade to allow it to move leftward. As shown in Fig.5a, the powders started to be spread onto the working plate. With the blade sliding leftward, the deposited powders formed a packed layer (Fig.5b). When the blade approached the left-boundary, that is, wall-1 (Fig.5c), powders were squeezed between wall-1 and the blade (Fig.5d), and non-deposited powders were scrolled downward to the trash zone and discarded. When the blade reached the top of wall-1, the powder layer in the working zone was formed.

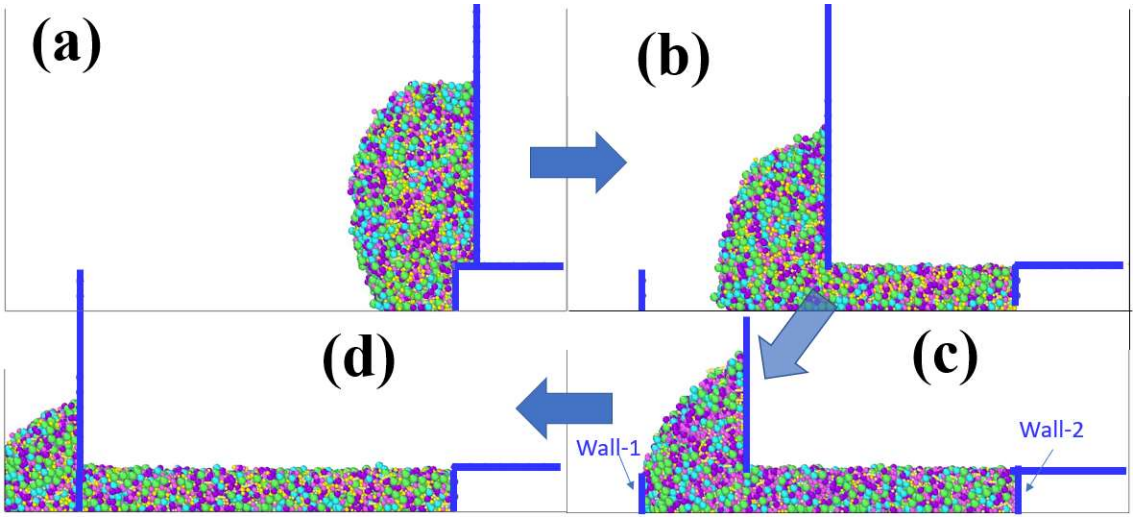

Fig.5. Snapshot views of the blade sliding process at different stages as (a) to (d).

Multiple blade sliding processes were carried out by varying the sliding speed from 0.01 to 0.5 m/s for 90-5-5 model (0.01m/s was only applied for the 90-5-5 model). Fig.6a shows the front views of the powder packing layer under six different sliding speeds. For easy presentation, the packing layer was divided into six lateral sections (along X-axis), in which section-VI was the first deposited and section-I was the last deposited. With a higher sliding speed, the powders were imposed with higher inertia of lateral speed, resulting in less powders to be spread onto the working plate, and thereby more loosely packed on the working plate, as shown in Fig.6b. Faster blade sliding also brought about a rougher top surface of the packing layer, especially at section-VI. For an individual PF curve, section-VI always had a lower PF than other sections. After passing section-VI, PF increased and became converged from section-V to section-II. With blade sliding approaching the end, quite a lot of powders were bounced back by wall-1, and being squeezed to pack tighter between wall-1 and blade, resulting in an

enhanced PF in section-I. Such PF trend across the six lateral sections was consistent across all the sliding speeds. In Fig.6b, the PF curves almost overlap under the sliding speeds of 0.05m/s and 0.01m/s, indicating PF became independent of sliding speed when sliding speed reduced to 0.05m/s and below.

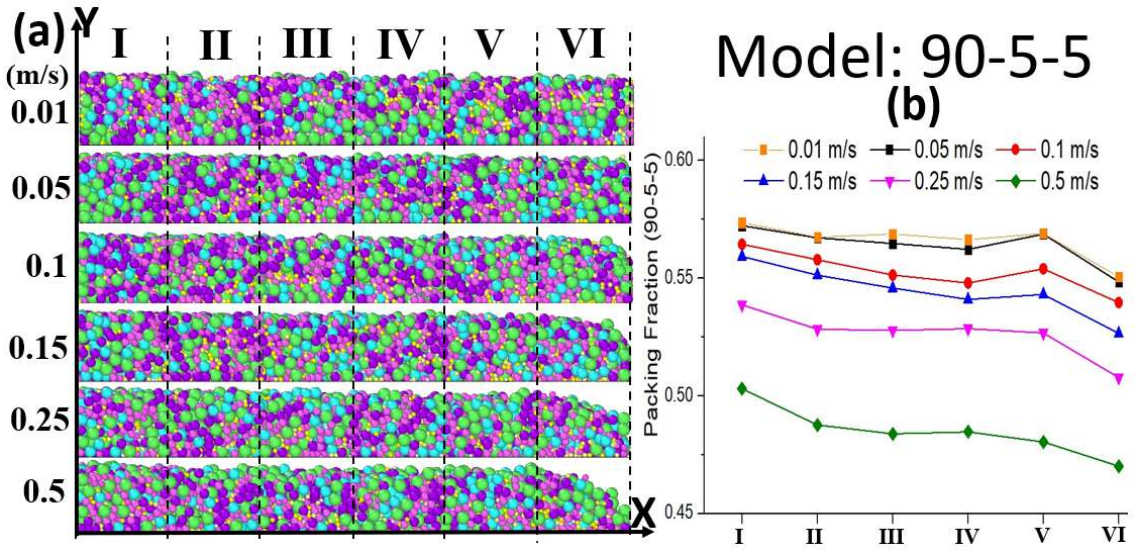

Fig.6. (a) Front view of the packing layer, and (b) PF plot, under different blade sliding speeds, for 90-5-5 model.

More plots for the simulation results from the 90-5-5 packing layer were shown in Fig.7. As discussed, more small-particles were in lower regions of the pouring heap, and they were likely to be spread onto the working plate earlier. As a result, in Fig.7a, the average diameter was the smallest in section-VI and increased leftward. In our observation, section-VI had less particles than section-V (Fig.7b), but a higher concentration of small-particles. Many small-particles agglomerated together without performing the gap-filling. Comparatively, section-V had more big-particles and comparable quantity of small-particles, in which the gap-filling became more prevalent, resulting in a higher PF than section-VI. It was noted that in section-V and section-VI (Fig.7a), slower sliding resulted in a lower average diameter, but an opposite relationship was observed at the commencement of section-IV. The mechanism lies in the fact that under slower sliding, most small-particles were spread into section-VI and section-V, and they became exhausted after the blade reached section-IV. Section-I had the largest value of average diameter as well as the highest number of particles due to the bouncing from wall-1.

As mentioned, in the pouring heap, the non-sphere-powders were normally at the lower positions and more likely to be spread earlier. This was clearly seen in Fig.7C and Fig.7D, in which slow sliding spread more STL and EPD powders in section-VI and section-V, and more in section-I due to bouncing from wall-1.

It was also noted that under fast sliding (blade sliding speed > 0.25m/s), more powders gained high-speed inertia and were directly swept into the trash wall, resulting in a much lower PF (Fig.6b). Therefore, from our investigation here, a sliding speed not exceeding 0.15 m/s is recommended to ensure a high packing density.

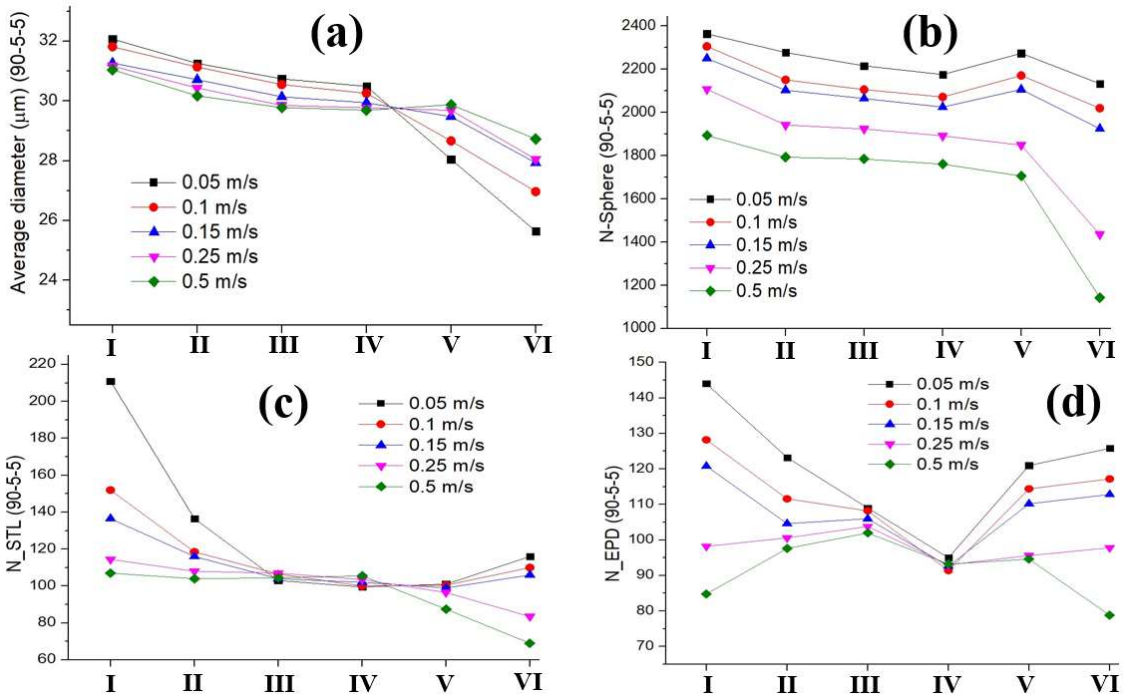

Fig.7. Plots for (a) average diameter (particles only), (b) number of particles, (c) number of STL powders and (d) number of EPD powders, for the 90-5-5 model under different sliding speeds.

For the 90-5-5 model, we studied more factors by varying their input parameters. Fig.8 presents the effects of particle-particle cohesion. From the snapshots of spreading (Fig.8a), it is seen clearly that after leaving the pouring plate, individual powders dropped in a discrete manner with a low cohesion but transferred to a cluster-falling manner with a strong cohesion. Accordingly, cluster spreading led to a lower and non-uniform distribution of PF (Fig.8b). When the cohesion reached 4 mJ/m^2, all the powders sticked together to form one block, and the spreading became impossible.

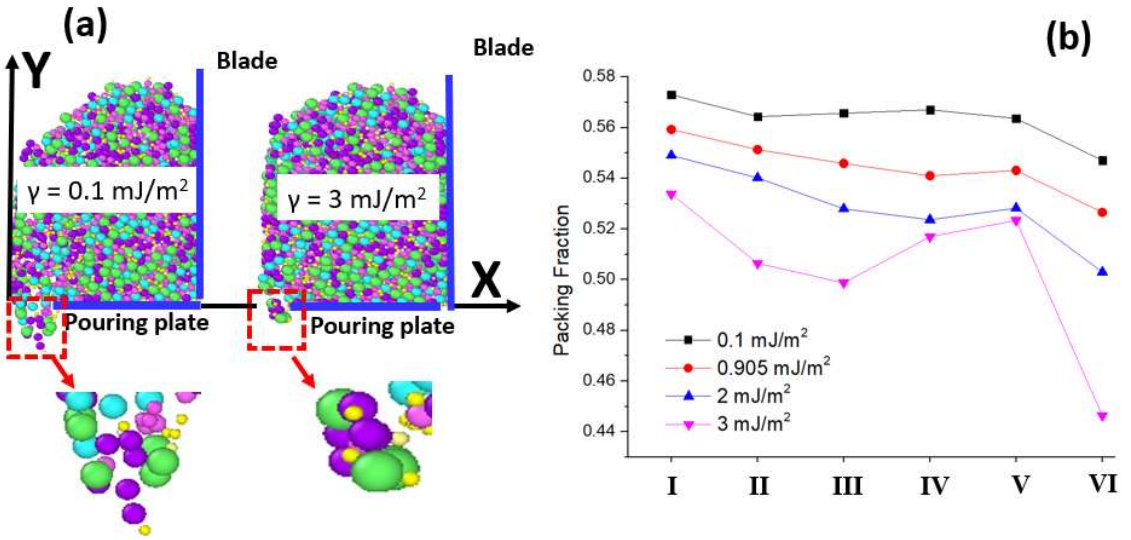

Fig.8. Particle-particle cohesion effect on the 90-5-5 model packing. (a) Snapshots of spread under different cohesions, and (b) PF plots under different cohesions.

Fig.9 shows the variation of PF with $\mu_{pp\text{-}s}$ (Fig.9a) and $\mu_{pp\text{-}r}$ (Fig.9b). After being spread onto the working plate, a lower friction resistance led to easy linear or rolling motions, and thus the powders gained higher flowability, and were more likely to reach minimum-energy positions, resulting in an enhancement in PF. Comparatively, the sliding friction ($\mu_{pp\text{-}s}$) imposed a stronger effect, which could result in a wide variation of PF (Fig.9a).

Both cohesion and friction were highly dependent on the surface condition, such as roughness, moisture, etc. Hence, it is important to keep smooth and dry surface of the powders to maintain sufficient flowability of individual powders during spreading process.

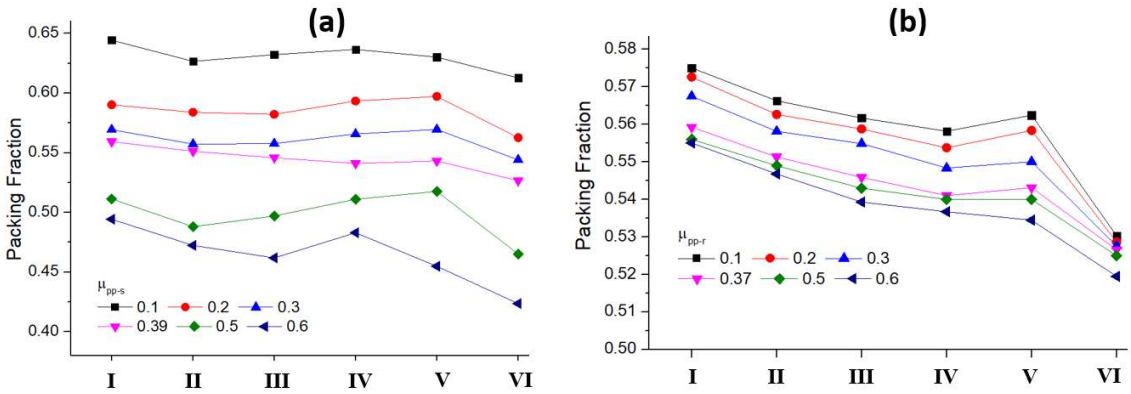

Fig.9. PF plots for 90-5-5 model with variation of COF parameters (a) $\mu_{pp\text{-}s}$, and (b) $\mu_{pp\text{-}r}$.

The front views and PF plots under different sliding speeds for a packing layer with the 40-30-30 and particle models were shown in Fig.10 and Fig.11, respectively. The observed characteristics and PF plots were similar to those of the 90-5-5 model (Fig.6). The differences in the PF values among three models were due to the differences in the powder types, which led to the differences in packing density and gap-filling effect.

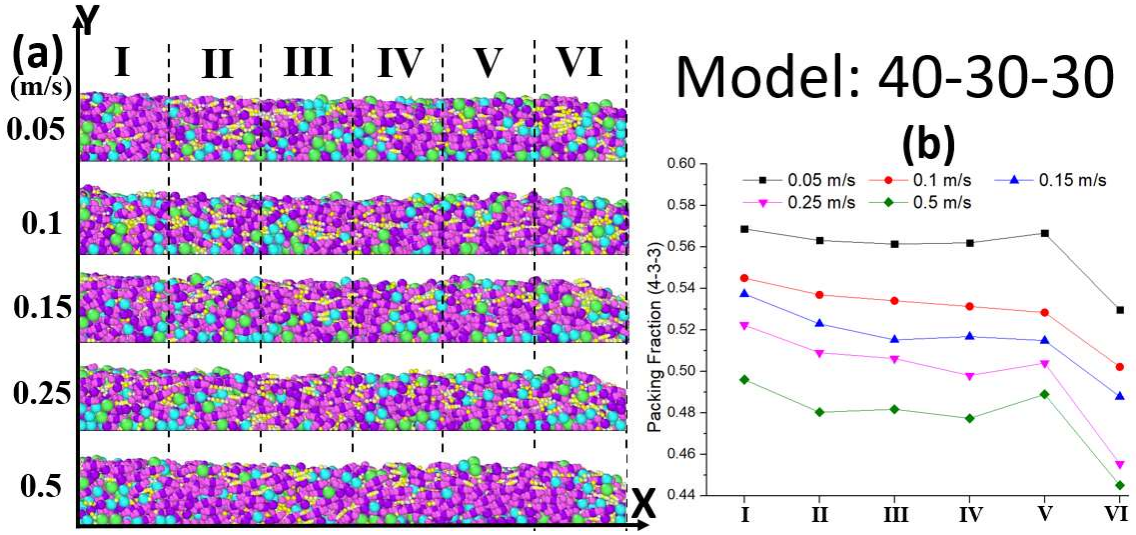

Fig.10. (a) Front view of the packing layer and (b) PF plot under different blade sliding speeds for the 40-30-30 model.

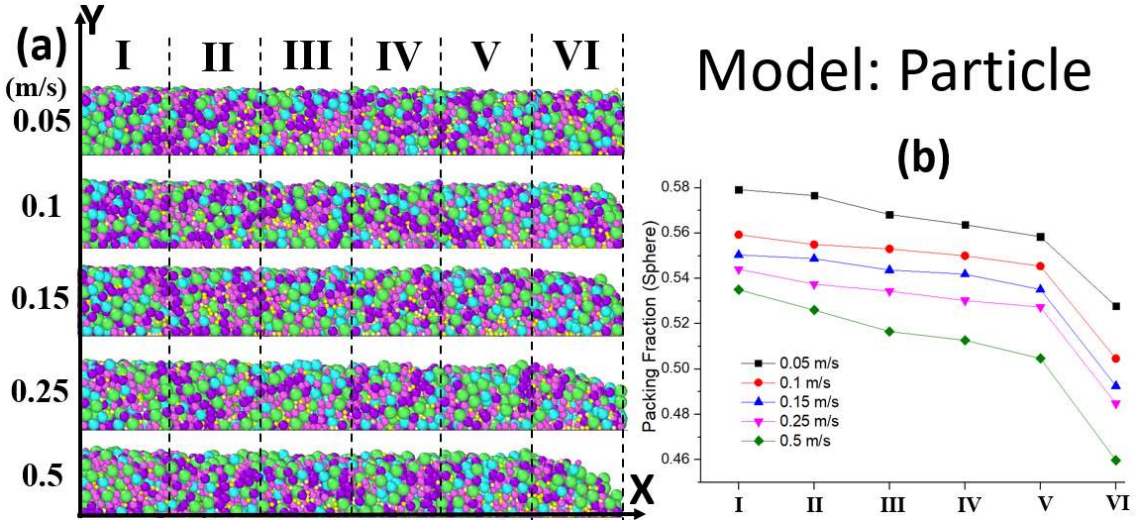

Fig.11. (a) Front view of the packing layer and (b) PF plot under different blade sliding speeds for the particle model.

3.3 Powder packing process improvement

It has been well established that PF of a random packing heap can reach an upper bound of PF around 0.64 [48]. However, with the typical spreading parameters, the PF of the 90-5-5 model could only reach around 0.56 (Fig.6b). In order to optimize the PF, here, we designed an improving two-step spread process, followed by a shaking process.

As shown in Fig.12, we separated particles as the small-particle group, and other as the non-small-particle group and the non-small-powder-group, as shown in Table-3. The quantities of powders for the two groups were shown in Table-1 for the 90-5-5 and particle models, and Gaussian size distribution was still applied for each individual group. With a 0.15 m/s blade sliding speed, the powders of the non-small-powders were spread onto

the working plate first (Fig.12a), followed by the 2nd blade sliding of the small-particles on top of the non-small-powder layer which were previously formed by the 1st blade sliding (Fig.12b), and the final deposited layer was named as BS-layer (Fig.12c). It can be seen that most of the small-particles were still located on the upper regions of the whole BS-layer. Upon the measurement, we found that the PF was slightly higher than that in Fig.6b, but still not satisfactory because the gap-filling effect was not well achieved.

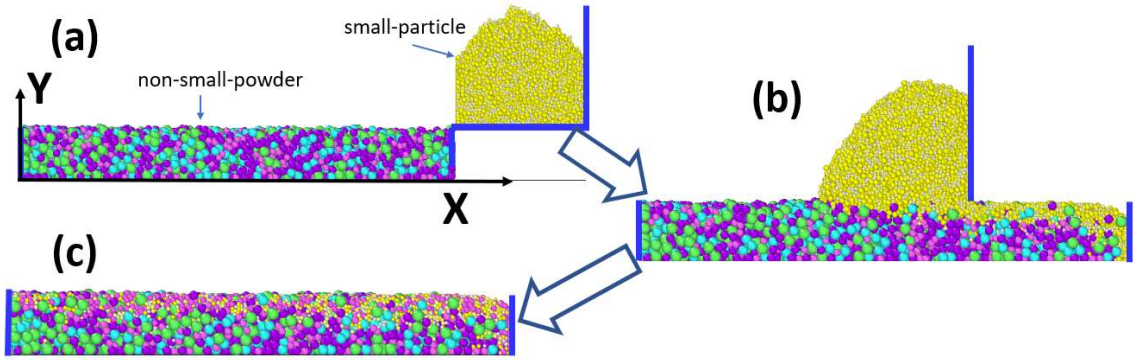

Fig.12. Two-step spread process of small-particles being spread onto the non-small-particle packing layer.

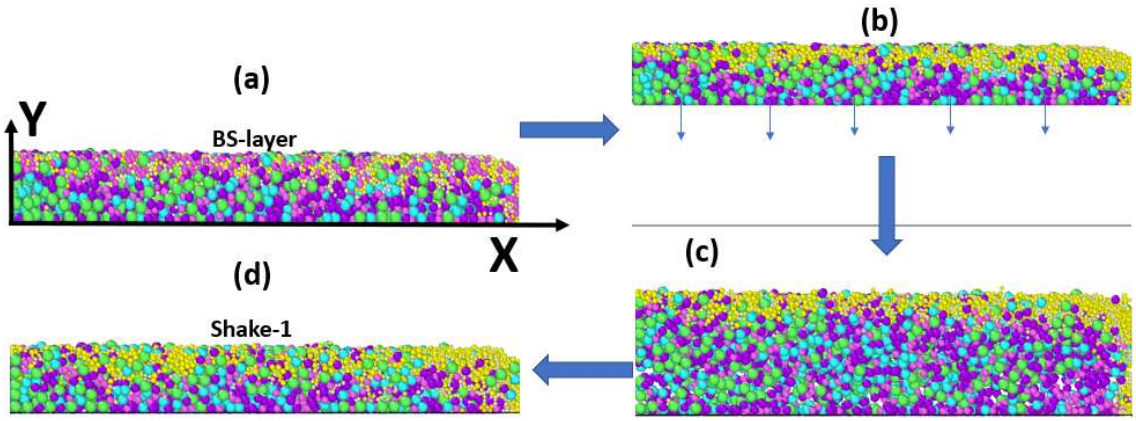

Fig.13. Cycle of shaking processes for the two-step spread model as (a) BS-layer, (b) powders were lifted to a height of 0.3mm and released to allow free-fall, (c) Falling powders hit the pouring plate and re-equilibrate, and (d) re-stabilized packing layer labelled as shake-1.

To further improve the PF and uniformity, subsequently, a shaking process was applied to the BS-layer. As shown in Fig.13, the BS-layer was firstly lifted by a height of 0.3mm (two times as its layer thickness), and then released (Fig.13b). The powders started to fall freely onto the working plate (Fig.13c). Those powder that touched working plate firstly would rebound from the plate, and collide with other falling powders, leading to re-mixing and "shaking" effect. Such re-mixing would re-equilibrate to form a new packing layer (shake-1). Such cycle of lift-fall-equilibrate was repeated five times for the 90-5-5 and particle models, whose cycle-wise views and PF plots were shown in Fig.14 and Fig.15.

During the lift-fall-equilibrate cycles, the packing morphology was re-organized, during which more pathways were opened between the non-small-powders so that small-particles were able to penetrate through from top to inner bulk. As shown in Fig.14a, with more cycles being carried out, more and more small-particles were observed to drift downward, indicating an enhanced gap-filling effect. Accordingly, in Fig.14b, the packing layer with only non-small-powders had the lowest PF of around 0.56 (section-II to section-IV), and it increased to around 0.59 after the spreading of the small-particles. The PF after one cycle of lift-fall-equilibrate significantly jumped to around 0.627. The PF kept increasing with more shaking cycles imposed. The plots for shake-4 and shake-5 were almost overlapping, indicating the attainment of the upper bound of PF, whose value was around 0.64, in agreement with the maximum PF for a random packing [48]. The enhanced PF was primarily attributed to the improved gap-filling effect. Besides PF, the good consistency between section-I and section-V also shows the enhancement in powder uniformity. Furthermore, as spotted in Fig.14a, after shake-5, more small-particles started to sink to the bottom regions, leading to vertical inhomogeneity. Thus, for the 90-5-5 model, the optimized process shall be a two-step spread, followed by 4 times shaking.

The particle model shows a very similar morphology and PF as the 90-5-5 model, and a 4 times shaking also reached the optimized PF. This means that a similar gap-filling effect could be achieved for the particle model, which suggests that the strategy of using lift-fall-equilibrate cycles is also effective even without the involvement of non-spherical powders. It is noted that if the shaking cycle keeps going on (more than 5 times), those small-particles will keep moving downward until entirely locating at the packing bottom, for which the PF will decrease and become non-mean along the height. Thus, there exists an optimal times of shaking, which is 4 times here.

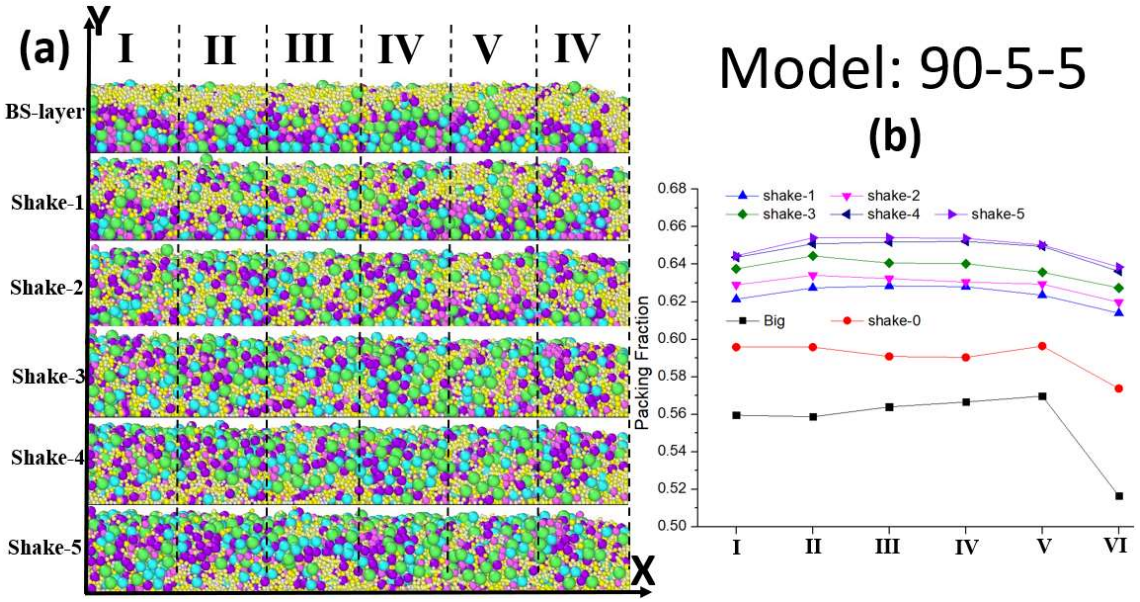

Fig.14. (a) Front views and (b) PF plots for BS-layer and each cycle of shaking process for the 90-5-5 model. The PF for the 1st spread of non-small-powders was also plotted for comparison.

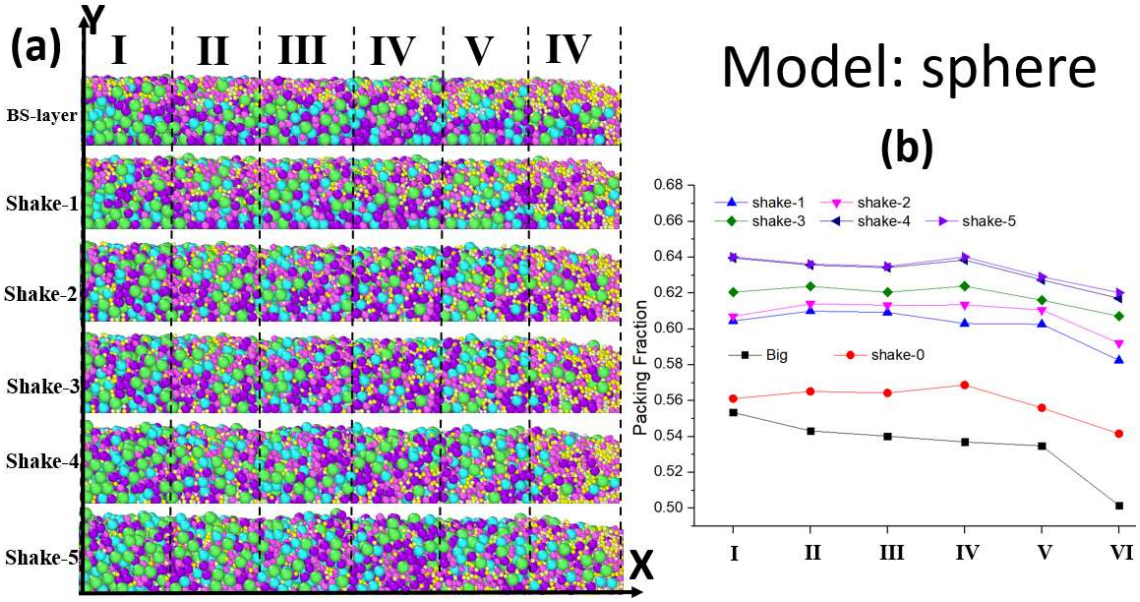

Fig.15. (a) Front views and (b) PF plots for BS-layer and each cycle of shaking process for the particle model. The PF for the 1st spread of non-small-powder was also plotted for comparison.

4. Conclusion

The major findings of our DEM simulations can be summarized as follows:

1) The inheritance from the pouring heap to the packing layer has been discovered. With random pouring, smaller and heavier powders were prone to occupy the lower regions of the pouring heap, which caused

a non-uniform distribution of powder types in the packing layer after blade sliding. Such size and shape segregation was not avoidable and needs to be understood.

2) It has been well established that a lower blade sliding rate was beneficial to packing density by multiple previous work reports. Meanwhile, based on our experimentally validated powder model, a sliding rate of 0.15m/s was recommended as the upper bound speed to achieve a high packing layer.
3) By tuning the particle-particle cohesion and friction, we observed a transition from the discrete to cluster deposition during blade spreading.
4) Non-spherical powders have been traditionally regarded as having a negative impact on packing density. In contrast, we found that a small portion of non-spherical powders (like in the ratio 90-5-5 in our study) can open more pathways for small particles to fill in the inner gaps, leading to an enhanced PF.
5) We proposed an improved process to achieve a high packing density and uniformity by using a two-step spreading followed by four times shaking. Such a procedure was found to increase PF to the upper bound, which is attributed to the enhanced gap-filling effect.

In summary, our work not only revealed fascinating mechanisms and insights into the powder packing process via blade sliding, but also introduced a novel strategy to improve powder packing density and uniformity in the powder layer. These advancements hold the potential to significantly improve the quality of additively manufactured components.

Compliance with Ethical Standards:

Funding: This study was funded by A*STAR (Agency for Science, Technology and Research, Singapore), under its RIE2025 Manufacturing, Trade and Connectivity (MTC) Industry Alignment Fund- Pre-Positioning (IAF-PP) "Metal AM Powders: Reusability, Rejuvenation, Cost, Quality & Performance (RRAMP) (Award M22K7a0047), grant SC23/21-1075EM ("Solid Solution, Short-range Ordering, Precipitation and Grain Boundary Strengthening Mechanisms and Their Impacts on the Mechanical and Chemical Properties of Medium Entropy Alloys: A Computational Study"), and the MTC Programmatic Fund through Grant M22L2b0111 ("Advanced Models for Additive Manufacturing").

Conflict of Interest: The authors declare that they have no conflict of interest.

References

[1] E. Sachs, M. Cima, J. Cornie, D. Brancazio, J. Bredt, A. Curodeau, T.L. Fan, S. Khanuja, A. Lauder, J. Lee, S. Michaels, Three-Dimensional Printing : The Physics and Implications of Additive Manufacturing, CIRP Ann, 42 (1993) 257-260.

[2] X.B. Gong, T. Anderson, K. Chou, Review on Powder-based Electron Beam Additive Manufacturing Technology, Manufacturing Rev., 1 (2014) 2-12.

[3] S. Ziegelmeier, P. Christou, F. Wollecke, C. Tuck, R. Goodridge, R. Hague, E. Krampe, E. Wintermantel, An Experimental Study into the Effects of Bulk and Flow Behaviour of Laser Sintering Polymer Powders on Resulting Part Properties, J. Mater. Process. Technol., 215 (2015) 239-250.

[4] E.L. Li, Z.Y. Zhou, L. Wang, R.P. Zou, A.B. Yu, Particle Scale Modelling of Powder Recoating and Melt Pool Dynamics in Laser Powder Bed Fusion Additive Manufacturing: A Review, Powder Technol., 409 (2022) 117789.
[5] C. Kloss, C. Goniva, A. hage, S. Amberger, S. Pirker, Models, Algorithms and Validation for Opensource DEM and CFD-DEM, Prog. Comput. Fluid Dyn., 12 (2012) 140-152.
[6] A.W. Roberts, Particle Technology - Reflections and Horizons: An Engineering Perspective, Trans. IChemE., 76 (1998) 775-796.
[7] E.B. Herbold, O. Walton, M.A. Homel, Simulation of Powder Layer Deposition in Additive Manufacturing Processes Using the Discrete Element Method, in, Lawrence Livermore National laboratory, Lawrence Livermore National laboratory, 2015.
[8] E.J.R. Parteli, DEM Simulation of Particles of Complex Shapes using the Multisphere Method: Application for Additive Manufacturing, AIP Conf. Proc., 1542 (2013) 185-188.
[9] H.W. Mindt, M. Megahed, N.P. Lavery, M.A. Holmes, S.G.R. Brown, Powder Bed Layer Characteristics: The Overseen First-Order Process Input, Metall. Mater. Trans. A, 47A (2016) 3811-3822.
[10] Z.J. Li, M. Mizutani, Influence of Layer Thickness and Substrate Bed on the Void Fraction of Powder Layers for Laser Powder Bed Fusion Powder Technol., 418 (2023) 118293.
[11] W.G. Nan, M. Pasha, T. Bonakdar, A. Lopez, U. Zafar, S. Nadimi, M. Ghadiri, Jamming during Particle Spreading in Additive Manufacturing, Powder Technol., 338 (2018) 253-262.
[12] W.G. Nan, M. Ghadiri, Numerical Simulation of Powder Flow during Spreading in Additive Manufacturing, Powder Technol., 342 (2019) 801-807.
[13] Q.Q. Han, H. Gu, R. Setchi, Discrete Element Simulation of Powder Layer Thickness in Laser Additive Manufacturing, Powder Technol., 352 (2019) 91-102.
[14] T.M. Wischeropp, C. Emmelmann, M. Brandt, A. Pateras, Measurement of Actual Powder Layer Height and Packing Density in a Single Layer in Selective Laser Melting, Addit. Manuf., 28 (2019) 176-183.
[15] T. Liu, C.S. Lough, H. Sehhat, Y.M. Ren, P.D. Christofides, E.C. Kinzel, M.C. Leu, In-situ Infrared Thermographic inspection for local powder layer thickness measurement in laser powder bed fusion, Addit. Manuf., 55 (2022) 102783.
[16] Y. Mahmoodkhani, U. Ali, S.I. Shahabad, A.R. Kasinathan, R. Esmaeilizadeh, A. Keshavarzkermani, E. marzbanrad, E. Toyserkani, On the Measurement of Effective Powder Layer Thickness in Laser Powder-bed Fusion Additive Manufacturing of Metals, Prog. Addit. Manuf., 4 (2019) 109-116.
[17] E.J.R. Parteli, T. Poschel, Particle-based Simulation of Powder Application in Additive Manufacturing, Powder Technol., 288 (2016) 96-102.
[18] A.B. Spierings, M. Voegtlin, T. Bauer, K. Wegener, Powder Flowability characterisation methodology for powder-bed based metal additive manufacturing, Prog. Addit. Manuf., 1 (2016) 9-20.
[19] A. Strondl, O. Lyckfeldt, H. Brondin, U. Ackelid, Characterization and Control of Powder Properties for Additive Manufacturing, JOM, 67 (2015) 549-554.
[20] F.H. Yu, S. Zhang, G.Z. Zhou, Y. Zhang, W. Ge, Geometrically Exact Discrete-Element-Method (DEM) Simulation on the Flow and Mixing of Sphero-Cylinders in Horizontal Drums, Powder Technol., 336 (2018) 415-425.
[21] D.D. Gu, M.J. Xia, D.H. Dai, On the Role of Powder Flow Behavior in Fluid Thermodynamics and Laser Processability of Ni-based Composites by Selective Laser Melting, Int. J. Mach. Tools Manuf., 137 (2019) 67-78.
[22] Y.F. Zhao, Y.J. Cui, Y. Hasebe, H.K. Bian, K. Yamanaka, K. Aoyagi, T. Hagisawa, A. Chiba, Controlling Factors Determining Flowability of Powders for Additive Manufacturing: A Combined Experimental and Simulation Study, Powder Technol., 393 (2021) 482-493.
[23] X.J. Ye, Y.P. Li, Y.L. Ai, Y. Nie, Novel Powder Packing theory with bimodal particle size distribution-application in superalloy, Adv. Powder Technol., 29 (2018) 2280-2287.
[24] M. Krantz, H. Zhang, J. Zhu, Characterization of Powder Flow: Static and Dynamic Testing, Powder Technol., 194 (2009) 239-245.

[25] A.B. Spierings, N. Herres, G. Levy, Influence of the Particle size Distribution on Surface Quality and Mechanical Properties in Additive Manufactured Stainless Steel Parts, Rapid Prototyping J, 17 (2011) 195-202.
[26] H.J.H. Brouwers, Particle-size Distribution and Packing Fraction of Geometric Random Packings, Phys. Rev. E, 74 (2006) 031309.
[27] W.C. Xia, Role of Particle Shape in the Floatability of Mineral Particle: An Overview of Recent Advances, Powder Technol., 317 (2017) 104-116.
[28] P.A. Langston, M.A. Al-Awamleh, F.Y. Fraige, B.N. Asmar, Distinct Element Modelling of Non-Spherical Frictionless Particle Flow, Chem. Eng. Sci., 59 (2004) 425-435.
[29] K. Saleh, S. Golshan, R. Zarghami, A Review on Gravity Flow of Free-Flowing Granular solids in Silos - Basics and Practical Aspects, Chem. Eng. Sci., 192 (2018) 1011-1035.
[30] L.O. Heim, J. Blum, M. Preuss, H.J. Butt, Adhesion and Friction Forces between Spherical Micrometer-Sized Particles, Phys. Rev. Lett., 83 (1999) 3328.
[31] Y.F. Ma, T.M. Evans, N. Philips, N. Cunningham, Numerical Simulation of the Effect of Fine Fraction on the Flowability of Powders in Additive Manufacturing, Powder Technol., 360 (2020) 608-621.
[32] L. Si, T.F. Zhang, M.Y. Zhou, M.Y. Li, Y. Zhang, H.M. Zhou, Numerical Simulation of the Flow Behavior and Powder Spreading Mechanism in Powder Bed-based Additive Manufacturing, Powder Technol., 394 (2021) 1004-1016.
[33] S.B. Wu, Z.L. Lei, M. Jiang, J.W. Liang, B.W. Li, Y.B. Chen, Experimental Investigation and Discrete Element Modeling for Particle-scale Powder Spreading Dynamics in Powder-bed-fusion-based Additive Manufacturing, Powder Technol., 403 (2022) 117390.
[34] H. Chen, T. Cheng, Z.W. Li, Q.S. Wei, W.T. Yan, Is High-speed Powder Spreading Really Unfavourable for the Part Quality of Laser Powder Bed Fusion Additive Manufacturing?, Acta Materialia, 231 (2022) 117901.
[35] T. Cheng, H. Chen, Q. Teng, Q.S. Wei, In-situ Experiment tests and particulate simulations on powder paving process of additive manufacturing, Particuology, 74 (2023) 164-172.
[36] S. Haeri, Y. Wang, O. Ghita, J. Sun, Discrete Element Simulation and Experimental Study of Powder Spreading Process in Additive Manufacturing, Powder Technol., 306 (2016) 45-54.
[37] S. Haeri, Optimisation of Blade Type Spreaders for Powder Bed Preparation in Additive Manufacturing using DEM Simulations, Powder Technol., 321 (2017) 94-104.
[38] H. Chen, A.S. Wei, S.F. Wen, Z.W. Li, Y.S. Shi, Flow Behavior of Powder Particles in Layering Process of Selective Laser Melting: Numerical Modeling and Experimental Verification based on Discrete Element Method, Int. J. Mach. Tools Manuf., 123 (2017) 146-159.
[39] H. Chen, Q.S. Wei, Y.J. Zhang, F. Chen, Y.S. Shi, W.T. Yan, Powder-spreading Mechanisms in Powder-bed-based Additive Manufacturing: Experiments and Computational Modeling, Acta Materialia, 179 (2019) 158-171.
[40] H. Chen, Y.X. Chen, Y. Liu, Q.S. Wei, Y.S. Shi, W.T. Yan, Packing Quality of Powder Layer during Counter-rolling-type Powder Spreading Process in Additive Manufacturing, blade, geometry, Int. J. Mach. Tools Manuf., 153 (2020) 103553.
[41] Y. He, A. Hassanpour, A.E. Bayly, Combined Effect of Particle Size and Surface Cohesiveness on Powder Spreadability for Additive Manufacturing, Powder Technol., 392 (2021) 191-203.
[42] D.Z. Yao, X.H. Liu, J. Wang, W. Fan, M. Li, H.T. Fu, H. Zhang, X.H. Yang, Q.C. Zou, X.Z. An, Numerical Insights on the Spreading of Practical 316 L Stainless Steel Powder in SLM Additive Manufacturing, Powder Technol., 390 (2021) 197-208.
[43] L. Wang, E.L. Li, H. Shen, R.P. Zou, A.B. Yu, Z.Y. Zhou, Adhesion Effects on Spreading of Metal Powders in Selective Laser Melting, Powder Technol., 363 (2020) 602-610.
[44] M.Y. Shaheen, A.R. Thornton, S. Luding, T. Weinhart, The Influence of Material and Pocess Parameters on Powder Spreading in Additive Manufacturing, Powder Technol., 383 (2021) 564-583.
[45] Q. Wu, C. Qiao, D.Z. Yao, X.Z. An, H. Zhang, H.T. Fu, X.H. Yang, Q.C. Zou, Research on Improving the Spreadability of Viscous Powder in Additive Manufacturing, Powder Technol., 413 (2023) 118061.

[46] Y.M. Fouda, A.E. Bayly, A DEM Study of Powder Spreading in Additive Layer Manufacturing, Granular Matter, 22:10 (2020).
[47] V. Lampitella, M. Trofa, A. Astarita, G. D'Avino, Discrete Element Method Analysis of the Spreading Mechanism and Its Influence on Powder Bed Characteristics in Additive Manufacturing, Micromachines, 12 (2021) 392.
[48] D.A. Weitz, Packing in the Spheres, Science, 303 (2004) 968-969.
[49] D. Dudzinski, A. Devillez, A. Moufki, D. Larrouquere, V. Zerrouki, J. Vigneau, A Review of Developments towards dry and high speed machining of Inconel 718 alloy, Int. J. Mach. Tool. Manu., 44 (2004) 439-456.
[50] L. Dai, Y.R. Chan, G. Vastola, Y.W. Zhang, Discrete Element Simulation of Powder Flow in Revolution Powder Analyser: Effects of Shape Factor, Friction and Adhesion, Powder Technol., 408 (2022) 117790.
[51] GE additive, https://www.ge.com/additive/.
[52] J.Y. Zhu, Y.Y. Liang, Y.H. Zhou, The Effect of the Particle Aspect Ratio on the Pressure at the Bottom of Sandpiles, Powder Technol., 234 (2013) 37-45.
[53] A.D. Renzo, F.P.D. Maio, Comparison of Contact-force Models for the Simulation of Collisions in DEM-based Granular Flow Codes, Chem. Eng. Sci., 59 (2004) 525-541.
[54] A.D. Renzo, F.P.D. Maio, An Improved Integral Non-linear Model for the Contact of Particles in Distinct Element Simulations, Chem. Eng. Sci., 60 (2005) 1303-1312.
[55] J. Ai, J.F. Chen, J.M. Rotter, J.Y. Ooi, Assessment of Rolling Resistance Models in Discrete Element Simulations, Powder Technol., 206 (2011) 269-282.
[56] L. Dai, Y.R. Chan, G. Vastola, N. Khan, S. Raghavan, Y.W. Zhang, Characterizing the Intrinsic Properties of Powder – A Combined Discrete Element Analysis and Hall Flowmeter Testing Study, Adv. Powder Technol., 32 (2021) 80-87.
[57] H. Kruggel-Emden, E. Simsek, S. Richelt, S. Wirtz, V. Scherer, Review and Extension of Normal Force Models for the Discrete Element Method, Powder Technol., 171 (2007) 157-173.
[58] J. Schafer, S. Deppel, D. Wolf, Force Schemes in Simulations of Granular Materials, J. de Physique, 6 (1996) 5-20.
[59] M. Combarros, H.J. Feise, H. Zetzener, A. Kwade, Segregation of Particulate Solids: Experiments and DEM Simulations, Particuology, 12 (2014) 25-32.
[60] M. Combarros Garcia, H.J. Feise, S. Strege, A. Kwade, Segregation in heaps and silos: Comparison between experiment, simulation and continuum model, Powder Technology, 293 (2016) 26-36.
[61] C. Meier, R. Weissbach, J. Weinberg, W.A. Wall, A.J. Hart, Modeling and Characterization of Cohesion in Fine Metal Powders with a Focus on Additive Manufacturing Process Simulations, Powder Technol., 343 (2019) 855-866.
[62] A. Phua, C. Doblin, P. Owen, C.H.J. Davies, G.W. Delaney, The Effect of Recoater Geometry and Speed on Granular Convection and Size Segregation in Powder Bed Fusion, Powder Technol., 394 (2021) 632-644.
[63] L. Dai, V. Sorkin, G. Vastola, Y.W. Zhang, Dynamics Calibration of Particle Sandpile Packing Characteristics via Discrete Element Method, Powder Technol., 347 (2019) 220-226.